Passivity-Based Control of Grid Forming and Grid Following Converters in Microgrids

Yonghao Gui, *Senior Member, IEEE*, Yaosuo Xue, *Senior Member, IEEE*
Electrification and Energy Infrastructures Division
Oak Ridge National Laboratory
Knoxville, United States
guiy@ornl.gov, xuey@ornl.gov

***Abstract*—With the integration of more and more power electronics devices into the grid, it is not easy to guarantee the stability of the whole system due to the complexity of the control structure of various power converters. In this paper, we consider grid-forming and grid-following converters in one microgrid, in which the grid-forming converters support the voltage and frequency of the microgrid and the grid-following converters inject their maximum power into the microgrid. To handle the stability issue, the passivity principle is applied to guarantee the stability of the whole microgrid. We ensure every grid-following converter satisfies the passivity via the port-controlled Hamiltonian method. In addition, we apply the passivity-based proportional-resonant controller to the grid-forming converter. One of the advantages of the proposed method is that the phase lock loop system is eliminated, which may cause stability issues. Simulation results show that the proposed method can control the microgrid effectively.**

***Index Terms*—Grid-forming, grid-following, microgrid, passivity, port-controlled Hamiltonian.**

I. Introduction

Increasing the penetration level of renewable energy sources such as solar photovoltaic (PV) and wind in the grid is an upward trend due to the goal of emissions reduction. Renewable energy sources are commonly integrated into the grid via power electronics devices, namely voltage source converters (VSCs). The control of VSC can be classified into two categories, namely grid-following control and grid-forming control [1]

Most renewable energy-based VSCs are operated in a grid-following mode to follow the frequency and voltage at the point of common coupling (PCC). For the conventional grid-following control VSCs, a phase lock loop (PLL) system is used to synchronize VSC with the grid at the PCC. It is not easy to guarantee the stability of the grid-following converters in a weak grid, i.e., when the grid impedance is very high, since the injected current and the PLL dynamics may cause instability issues under disturbances [2], [3]. Various scholars analyzed the stability via linear methods based on impedance or admittance [4]. The linear techniques indicate that the VSCs are stable around an existing stable equilibrium point under the disturbance. However, it is not easy to guarantee stability under large disturbances.

To solve this issue, grid-forming controls are deployed. Virtual synchronous generator [5], droop control [6], [7], virtual oscillator [8], [9], and robust method [10] are used to operate the VSCs in grid-forming controls in order to improve stability. However, different types of grid-forming controls lead to different stability issues in the grid [11]. A large signal stability analysis method is presented for grid-forming and grid-following VSCs considering disturbance (fault) by using Lyapunov stability theory and La Salle's Invariance Principle [12]. It can find a stability boundary for certain operating points of grid-forming and grid-following VSCs. However, local stability can be guaranteed, and it is not easy to analyze the stability of the whole system if more and more VSCs are integrated into the grid.

To solve this issue, the passivity principle is applied to guarantee the stability of the whole grid, where if the passive sub-systems in the microgrid are integrated into parallel or feedback, the entire grid is also passive and stable [13]. One of the popular methods is a port-controlled Hamiltonian method, which is widely used in various applications to guarantee passivity property [14], [15]. Hence, we ensure every VSCs operating in the grid satisfies the passivity. In this paper, we consider a small microgrid with different types of distributed energy resources (DERs), e.g., energy storage system (ESS), wind turbine (WT), and PV. Since grid-forming VSCs are capable of changing their output faster to fix the frequency of the microgrid in the case of load-shedding or renewable DERs variation [16], an ESS is controlled in a grid-forming mode to support the voltage and frequency of the microgrid. Then, other renewable DERs are controlled in the grid-following mode to inject their maximum power into the microgrid. To satisfy the passivity requirement, we use the port-controlled Hamiltonian method for the grid-following VSCs to get the passivity property. In addition, to eliminate the PLL, which may cause some stability issues, we control the grid-following VSCs through a voltage-modulated direct power control method, which has been successfully applied in many applications [17]–[22]. For the grid-forming VSCs, we

use the proportional-resonant (PR) controller. Consequently, the PLL is eliminated in the grid-following or grid-forming VSCs. Simulation results show that the proposed method can control the VSCs in the microgrid effectively.

II. Control of Power Electronics Based Sources

In this study, it is assumed that the ESS uses the grid-forming control to support the voltage and frequency of the microgrid, and the renewable DERs use the grid-following control to inject their maximum power into the microgrid. For the grid-forming control VSC, we use the PR controller designed in [23] and design the outer-loop controller using the voltage and frequency as the references to generate the reference of the inner-loop reference. For the grid-following control VSC, we modify the VM-DPC based on the port-controlled Hamiltonian method. Compared with the method in [24], the proposed method has a simple structure, which means it can be easily implemented.

A. Grid Following Converters

For the sake of simplicity, a balanced grid voltage condition is considered in this study. The instantaneous real power, P, and reactive power, Q, by using the line current and grid voltage in the α-β reference frame can be formulated as follows [25]:

$$\begin{aligned} P &= \frac{3}{2}(v_{o,\alpha}i_{o,\alpha} + v_{o,\beta}i_{o,\beta}), \\ Q &= \frac{3}{2}(v_{o,\beta}i_{o,\alpha} - v_{o,\alpha}i_{o,\beta}), \end{aligned} \tag{1}$$

where $v_{o,\alpha}$, $v_{o,\beta}$, $i_{o,\alpha}$, and $i_{o,\beta}$, indicate the grid voltages and line currents and in α–β reference frame, respectively. Based on the dynamics of the grid-connected converter with an L-filter [26], [27], the dynamics of the instantaneous real and reactive powers could be obtained using the grid voltage variations as follows:

$$\begin{aligned} \frac{dP}{dt} &= -\frac{R}{L}P - \omega Q + \frac{3}{2L}(v_{o,\alpha}v_{c,\alpha} + v_{o,\beta}v_{c,\beta} - V_g^2), \\ \frac{dQ}{dt} &= \omega P - \frac{R}{L}Q + \frac{3}{2L}(v_{o,\beta}v_{c,\alpha} - v_{o,\alpha}v_{c,\beta}), \end{aligned} \tag{2}$$

where $V_g = \sqrt{v_{o,\alpha}^2 + v_{o,\beta}^2}$. In (2), ω is the angular velocity of the grid voltage. $v_{c,\alpha}$ and $v_{c,\beta}$ are converter voltages in α–β reference frame, respectively. The VM-DPC control variables can be defined to obtain a simpler model as in [28]

$$\begin{aligned} u_P &:= v_{o,\alpha}v_{c,\alpha} + v_{o,\beta}v_{c,\beta} - V_g^2, \\ u_Q &:= v_{o,\beta}v_{c,\alpha} - v_{o,\alpha}v_{c,\beta}. \end{aligned} \tag{3}$$

Then, the system in (2) is changed into

$$\begin{aligned} \frac{dP}{dt} &= -\frac{R}{L}P - \omega Q + \frac{3}{2L}u_P, \\ \frac{dQ}{dt} &= \omega P - \frac{R}{L}Q + \frac{3}{2L}u_Q, \end{aligned} \tag{4}$$

Let us define two states and two control inputs as

$$x = \begin{bmatrix} x_1 \\ x_2 \end{bmatrix} = \begin{bmatrix} P \\ Q \end{bmatrix}, u = \begin{bmatrix} u_1 \\ u_2 \end{bmatrix}^T = \begin{bmatrix} u_P \\ u_Q \end{bmatrix}^T$$

Then, a state-space model of GFC is formulated such as

$$\begin{aligned} \dot{x} &= \begin{bmatrix} -\frac{R}{L}x_1 - \omega x_2 + \frac{3}{2L}u_1 \\ \omega x_1 - \frac{R}{L}x_2 + \frac{3}{2L}u_2 \end{bmatrix}, \\ y &= \begin{bmatrix} x_1 & x_2 \end{bmatrix}^T. \end{aligned} \tag{5}$$

where y is the output of the system.

It can be seen that the system is satisfied the port-controlled Hamiltonian form described in [14], [29]. In order to use the port-controlled Hamiltonian system, it is supposed that there exist signals u_d and x_d that satisfy the system in (5) [30].

Taking a Hamiltonian function for the grid-following control system in (5) as follows:

$$H(x) = \frac{1}{2}x^T S x, \tag{6}$$

where S is a 2 by 2 identity matrix.

$$\dot{x} = (\mathfrak{R} + \mathfrak{J})\frac{\partial H(x)}{\partial x} + G(u) \tag{7}$$

where

$$\begin{aligned} H(x) = \frac{1}{2}x^T S x \quad S &= \begin{bmatrix} 1 & 0 \\ 0 & 1 \end{bmatrix} \succ 0 \\ \mathfrak{R} = \mathfrak{R}^T &= \begin{bmatrix} -\frac{R}{L} & 0 \\ 0 & -\frac{R}{L} \end{bmatrix} \prec 0 \\ \mathfrak{J} = -\mathfrak{J}^T &= \begin{bmatrix} 0 & -\omega \\ \omega & 0 \end{bmatrix}, \; G(u) = \frac{3}{2L}\begin{bmatrix} u_1 \\ u_2 \end{bmatrix} \end{aligned}$$

The desired dynamics can be obtained as follows:

$$\dot{x}^d = (\mathfrak{R} + \mathfrak{J})\frac{\partial H(x^d)}{\partial x^d} + G(u^d). \tag{8}$$

Let's define the error as follows:

$$e = x^d - x.$$

Then, the error dynamics can be obtained as

$$\dot{e} = (\mathfrak{R} + \mathfrak{J})\frac{\partial H(e)}{\partial e} + G(u^d - u). \tag{9}$$

In order to guarantee the passivity by using the port-controlled Hamiltonian form, $H(e)$ is taken as a Lyapunov function candidate, then its derivative of $H(e)$ is obtained as follows:

$$\begin{aligned} \dot{H}(e) &= \frac{1}{2}\left(\dot{e}^T\left(\frac{\partial H(e)}{\partial e}\right) + \left(\frac{\partial H(e)}{\partial e}\right)^T\dot{e}\right) \\ &= e^T S^T \mathfrak{R} S e + G(u^d - u)e \end{aligned} \tag{10}$$

If taking a controller such that

$$u = u^d + e^T K \tag{11}$$

where K is the controller gain, then, (10) is changed into

$$\dot{H}(e) = e^T(S^T\mathfrak{R}S - \frac{3}{2L}K)e \tag{12}$$

In (12), $\mathfrak{R}$ is a negative definite matrix, thus the closed-loop system is exponentially stable if K is taken as a positive definite matrix by using the port-controlled Hamiltonian method. Furthermore, K can be tuned for the convergence

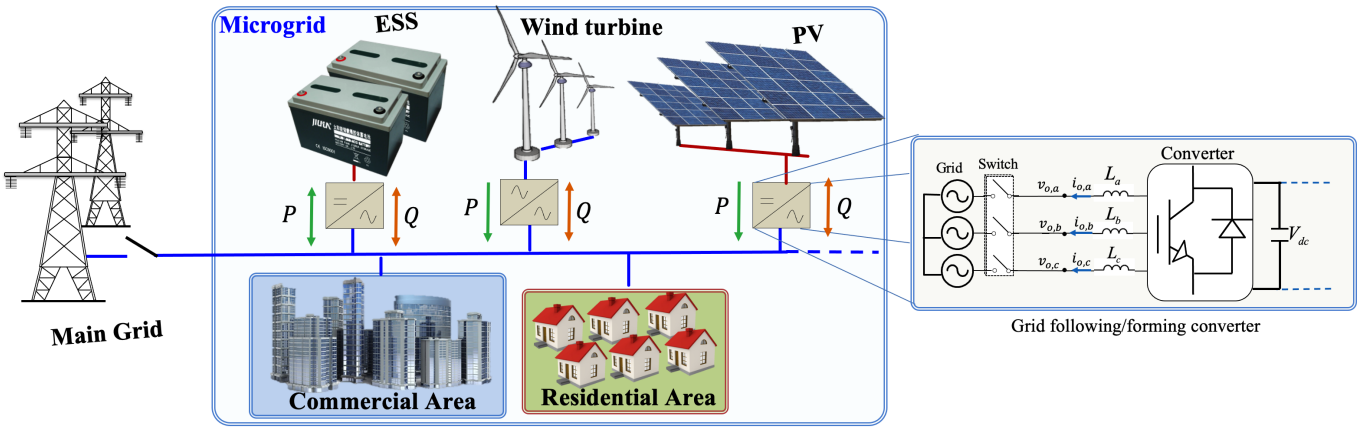

Fig. 1. Grid architecture with energy storage system, renewable energy sources (PV and wind turbine), and loads.

rate of the system. It should be noted that the controller K is a proportional controller, but it can be replaced by a proportional-integral controller in the implementation in order to reduce errors when there exist uncertainties in the practical system. The stability analysis of the closed-loop system with the proportional-integral controller is omitted due to the page limit.

From (11), it can be seen that u^d is the core part of the control input. Generally, the references of the outputs are given or can be calculated by using the maximum power point tracking (MPPT) control strategy for P^* and the grid voltage controller for Q^*. For the sake of simplicity, it is assumed that the references of the outputs are given in this study, i.e., y^d is given. Consequently, the desired control input u^d can be calculated by using the flatness property [31] by using (4) as follows:

$$u^d = \begin{bmatrix} u_1^d \\ u_2^d \end{bmatrix} = \begin{bmatrix} \frac{2L}{3}\dot{y}_1^d + \frac{2R}{3}y_1^d + \frac{2L\omega}{3}y_2^d \\ \frac{2L}{3}\dot{y}_2^d - \frac{2L\omega}{3}y_1^d + \frac{R}{L}y_2^d \end{bmatrix}. \tag{13}$$

Finally, the control input is generated by using (11) and (13). The original input can be calculated as follows:

$$\begin{bmatrix} v_{c,\alpha} \\ v_{c,\beta} \end{bmatrix} = \begin{bmatrix} \frac{v_{o,\alpha}u_1 + v_{o,\beta}u_2}{V_g^2} + v_{o,\alpha} \\ \frac{v_{o,\beta}u_1 - v_{o,\alpha}u_2}{V_g^2} + v_{o,\beta} \end{bmatrix}. \tag{14}$$

that is used for pulse width modulation (PWM) to generate the switching signals for VSC as shown in Fig. 2. Based on the proposed method, it can guarantee the passivity of the grid-following VSCs.

B. Grid Forming Converters

In this study, the VSC of ESS is operated at grid-forming mode to support the voltage and frequency of the microgrid. To guarantee the passivity and exclude the PLL system, the controller designed in [23] is used in this study, which was designed in the α-β reference frame. The control input of the VSC of ESS can be generated as

$$v^*_{\mathrm{v},\alpha\beta} = -F(s)\left(i^*_{v,\alpha\beta} - i_{v,\alpha\beta}\right) + H_m(s)\left(i_{c,\alpha\beta} - i_{v,\alpha\beta}\right) \tag{15}$$

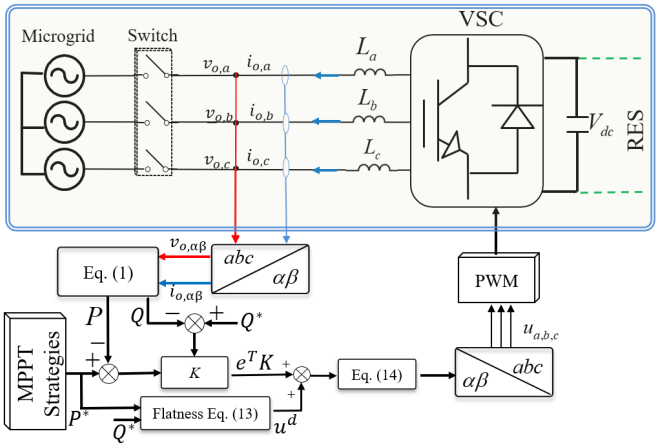

Fig. 2. Control block diagram of the grid-following VSCs.

where

$$F(s) = \alpha_c L + F_{R_h}(s), \quad H_m(s) = \frac{sKH_c(s)}{sC_g}$$

In (15), $v^*_{\mathrm{v},\alpha\beta}$ is the reference voltage of converter used in the PWM. $i_{v,\alpha\beta}$ and $i^*_{v,\alpha\beta}$ are the VSC side current and its reference in the α-β reference frame, respectively. $i_{c,\alpha\beta}$ is the capacitor current in the α-β reference frame. $F_{R_h}(s)$ is a general R part for a harmonic of order h, and $H_c(s)$ is a biquad filter satisfying phase lag or lead at certain frequency. The PR controller in (15) adds a modified active damping with a compensation filter to guarantee passivity. The detailed parameter selection can be found in [23]. Consequently, we can apply another PR controller for the voltage control loop to generate the current reference in the inner loop. The control block diagram can be found in Fig. 3.

III. Performance Validation

The proposed method is validated in a microgrid through MATLAB/Simulink Simscape Electrical model. The microgrid consists of one ESS, WT, PV, and two loads. The system parameters used in the simulation are listed as Table I.

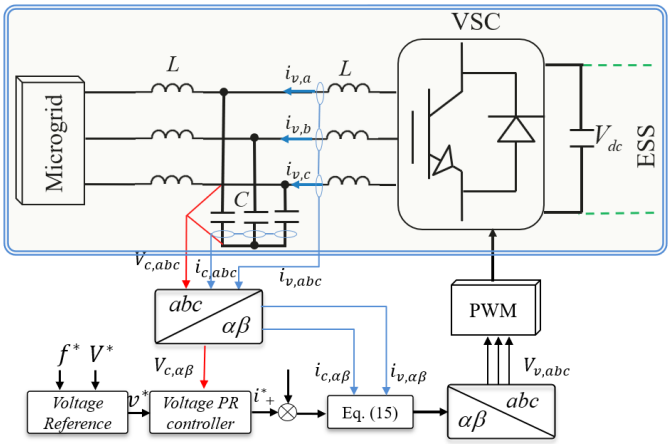

Fig. 3. Control block diagram of the grid-forming VSC.

TABLE I
SYSTEM PARAMETERS IN THE CASE STUDY

Parameter	Symbol	Value
Nominal grid voltage	V^*_{rms}	230 V
Nominal grid frequency	f^*	50 Hz
Filter inductance of ESS	L_{in}	1.8 mH
Output inductance of ESS	L_o	1.8 mH
Filter capacitor of ESS	C	27 μF
Filter inductance of PV & WT	L_{pv}&L_{wt}	6 mH
Switching frequency of VSCs	f_{sw}	10 kHz

Fig. 4 and Fig. 5 show the simulation results of the case study. At first, the ESS supports the voltage and frequency of the microgrid when there is a load connected to the microgrid. At 5.1 s, the WT is connected and injects the same power as the load. Consequently, the ESS reduces its output power to zero autonomously since the additional generation from the WT increases the microgrid frequency as shown in Fig. 5. After 2 seconds, the PV is connected and generates its maximum power. Since the generation power is larger than the consumption, the ESS starts to charge the surplus power to keep the balance of the generation and load. Finally, at 1 s, an additional load is connected and the total load equals the generation of WT and PV. Hence, the output power of ESS is zero but it still supports the voltage and frequency of the microgrid as shown in Fig. 4. In addition, the voltage and frequency of the microgrid are controlled by the ESS without losing stability. It can be concluded that the proposed method can manage the microgrid effectively.

IV. Conclusions and Future Works

A passivity-based control of grid-forming and grid-following VSCs in a microgrid was presented in this paper, where the grid-forming VSC supports the voltage and frequency of the microgrid and the grid-following VSCs follow their MPPT. An advantage of the proposed method is that the stability of the whole microgrid is guaranteed via the passivity principle. Another advantage is that the phase lock loop system is eliminated for instability issues. Simulation results show that the proposed method can control the microgrid effectively.

In the future, the proposed method will be extended to all power electronics grids in order to guarantee the stability of the whole grid. In addition, the state of charge will be considered to avoid the loss of the grid-forming converter in the microgrid.

Acknowledgments

This material is based upon work supported by the US Department of Energy, Office of Electricity, Advanced Grid Modeling Program under contract DE-AC05-00OR22725.

References

[1] J. Rocabert, A. Luna, F. Blaabjerg, and P. Rodriguez, "Control of power converters in AC microgrids," *IEEE Trans. Power Electron.*, vol. 27, no. 11, pp. 4734–4749, 2012.

[2] D. Dong, B. Wen, D. Boroyevich, P. Mattavelli, and Y. Xue, "Analysis of phase-locked loop low-frequency stability in three-phase grid-connected power converters considering impedance interactions," *IEEE Trans. Ind. Electron.*, vol. 62, no. 1, pp. 310–321, 2015.

[3] X. Wang, H. Wu, X. Wang, L. Dall, and J. B. Kwon, "Transient stability analysis of grid-following VSCs considering voltage-dependent current injection during fault ride-through," *IEEE Trans. Energy Convers.*, pp. 1–13, 2022, DOI: 10.1109/TEC.2022.3204358.

[4] S. Gao, H. Zhao, P. Wang, Y. Gui, V. Terzija, and F. Blaabjerg, "Comparative study of symmetrical controlled grid-connected inverters," *IEEE Trans. Power Electron.*, vol. 37, no. 4, pp. 3954–3968, 2022.

[5] M. Chen, D. Zhou, and F. Blaabjerg, "Enhanced transient angle stability control of grid-forming converter based on virtual synchronous generator," *IEEE Trans. Ind. Electron.*, vol. 69, no. 9, pp. 9133–9144, 2022.

[6] J. W. Simpson-Porco, F. Dörfler, and F. Bullo, "Synchronization and power sharing for droop-controlled inverters in islanded microgrids," *Automatica*, vol. 49, no. 9, pp. 2603–2611, 2013.

[7] L. Huang *et al.*, "Transient stability analysis and control design of droop-controlled voltage source converters considering current limitation," *IEEE Trans. Smart Grid*, vol. 10, no. 1, pp. 578–591, 2019.

[8] M. Li, Y. Gui, Y. Guan, J. Matas, J. M. Guerrero, and J. C. Vasquez, "Inverter parallelization for an islanded microgrid using the Hopf oscillator controller approach with self-synchronization capabilities," *IEEE Trans. Ind. Electron.*, vol. 68, no. 11, pp. 10 879–10 889, 2021.

[9] L. Kong, Y. Xue, L. Qiao, and F. Wang, "Enhanced synchronization stability of grid-forming inverters with passivity-based virtual oscillator control," *IEEE Trans. Power Electron.*, vol. 37, no. 12, pp. 14 141–14 156, 2022.

[10] M. Chen, D. Zhou, A. Tayyebi, E. Prieto-Araujo, F. Dörfler, and F. Blaabjerg, "Generalized multivariable grid-forming control design for power converters," *IEEE Trans. Smart Grid*, vol. 13, no. 4, pp. 2873–2885, 2022.

[11] X. He, S. Pan, and H. Geng, "Transient stability of hybrid power systems dominated by different types of grid-forming devices," *IEEE Trans. Energy Convers.*, vol. 37, no. 2, pp. 868–879, 2021.

[12] X. Fu *et al.*, "Large-signal stability of grid-forming and grid-following controls in voltage source converter: A comparative study," *IEEE Trans. Power Electron.*, vol. 36, no. 7, pp. 7832–7840, 2021.

[13] H. K. Khalil, *Nonlinear control*. Pearson New York, 2015, vol. 406.

[14] H. Sira-Ramirez and Silva-Ortigoza, *Control design techniques in power electronics devices*. Springer-Verlag London Limited, 2006.

[15] Y. Gui, C. Kim, and C. C. Chung, "Improved low-voltage ride through capability for PMSG wind turbine based on port-controlled Hamiltonian system," *Int. J. Control Autom. Syst.*, vol. 14, no. 5, pp. 1195–1204, 2016.

[16] R. H. Lasseter, Z. Chen, and D. Pattabiraman, "Grid-forming inverters: A critical asset for the power grid," *IEEE J. Emerg. Sel. Topics Power Electron.*, vol. 8, no. 2, pp. 925–935, 2020.

[17] S. Gao, H. Zhao, Y. Gui, D. Zhou, V. Terzija, and F. Blaabjerg, "A novel direct power control for DFIG with parallel compensator under unbalanced grid condition," *IEEE Trans. Ind. Electron.*, vol. 68, no. 10, pp. 9607–9618, 2021.

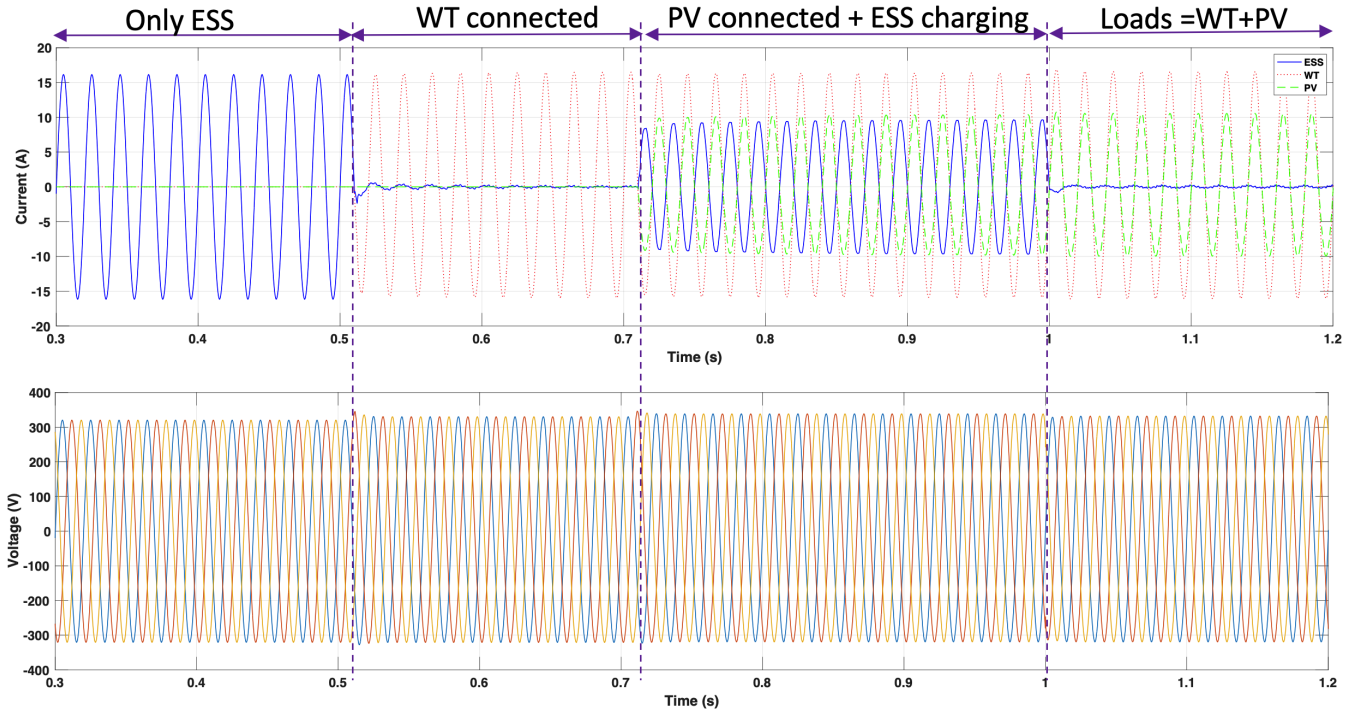

Fig. 4. Simulation results. (top) Currents of ESS, WT, and PV; (bottom) microgrid voltage.

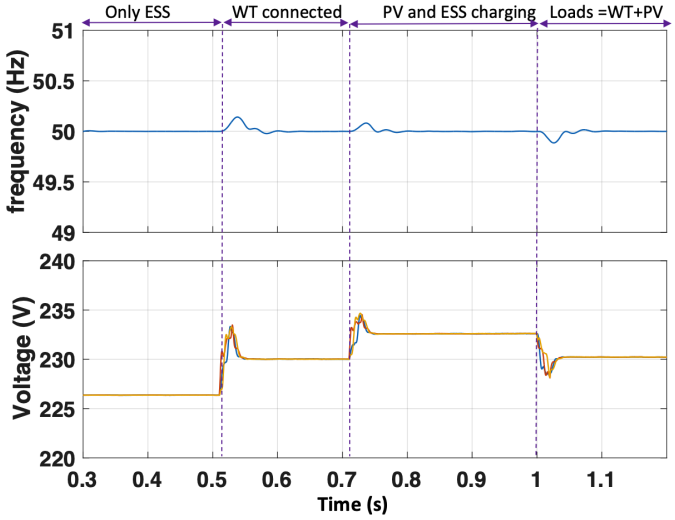

Fig. 5. Simulation results. (top) frequency of microgrid, (bottom) RMS voltage of microgrid.

[18] R.-J. Wai and Y. Yang, "Design of backstepping direct power control for three-phase PWM rectifier," *IEEE Trans. Ind. Appl.*, vol. 55, no. 3, pp. 3160–3173, 2019.

[19] Y. Gui, X. Wang, and F. Blaabjerg, "Vector current control derived from direct power control for grid-connected inverters," *IEEE Trans. Power Electron.*, vol. 34, no. 9, pp. 9224–9235, 2019.

[20] F. Mazouz, S. Belkacem, I. Colak, S. Drid, and Y. Harbouche, "Adaptive direct power control for double fed induction generator used in wind turbine," *Int. J. Electr. Power Energy Syst.*, vol. 114, p. 105395, 2020.

[21] Z. Gong, C. Liu, L. Shang, Q. Lai, and Y. Terriche, "Power decoupling strategy for voltage modulated direct power control of voltage source inverters connected to weak grids," *IEEE Trans. Sustain. Energy*, pp. 1–15, 2022, doi: 10.1109/TSTE.2022.3204405.

[22] Z. Gong, C. Liu, Y. Gui, F. F. da Silva, and C. L. Bak, "Power decoupling method for voltage source inverters using grid voltage modulated direct power control in unbalanced system," *IEEE Trans. Power Electron.*, pp. 1–16, 2022, doi: 10.1109/TPEL.2022.3220436.

[23] L. Harnefors, A. G. Yepes, A. Vidal, and J. Doval-Gandoy, "Passivity-based controller design of grid-connected VSCs for prevention of electrical resonance instability," *IEEE Trans. Ind. Electron.*, vol. 62, no. 2, pp. 702–710, 2015.

[24] Y. Gui, B. Wei, M. Li, J. M. Guerrero, and J. C. Vasquez, "Passivity-based coordinated control for islanded ac microgrid," *Appl. energy*, vol. 229, pp. 551–561, 2018.

[25] F. Z. Peng and J.-S. Lai, "Generalized instantaneous reactive power theory for three-phase power systems," *IEEE Trans. Instrum. Meas.*, vol. 45, no. 1, pp. 293–297, 1996.

[26] J. Hu, "Improved dead-beat predictive DPC strategy of grid-connected DC–AC converters with switching loss minimization and delay compensations," *IEEE Trans. Ind. Informat.*, vol. 9, no. 2, pp. 728–738, 2013.

[27] Y. Gui, C. Kim, C. C. Chung, J. M. Guerrero, Y. Guan, and J. C. Vasquez, "Improved direct power control for grid-connected voltage source converters," *IEEE Trans. Ind. Electron.*, vol. 65, no. 10, pp. 8041–8051, Oct 2018.

[28] Y. Gui, X. Wang, H. Wu, and F. Blaabjerg, "Voltage-modulated direct power control for a weak grid-connected voltage source inverters," *IEEE Trans. Power Electron.*, vol. 34, no. 11, pp. 11 383–11 395, 2019.

[29] Y. Gui, C. C. Chung, F. Blaabjerg, and M. G. Taul, "Dynamic extension algorithm-based tracking control of STATCOM via port-controlled Hamiltonian system," *IEEE Trans. Ind. Inform.*, vol. 16, no. 8, pp. 5076–5087, 2020.

[30] Y. Gui, D. E. Chang, and C. C. Chung, "Tracking controller design methodology for passive port-controlled Hamiltonians with application to type-2 STATCOM systems," in *Proc. IEEE Conf. Decis. Control, Italy*, 2013, pp. 1653–1658.

[31] J. Levine, *Analysis and control of nonlinear systems: A flatness-based approach*. Springer Science & Business Media, 2009.